Optical Materials: X 16 (2022) 100188

Contents lists available at ScienceDirect

Optical Materials: X

journal homepage: www.journals.elsevier.com/optical-materials-x

The d-d transitions and ligand field parameters for Cr^{3+}/Co^{2+} doped (Mg, Zn)Al_2O_4: Multi-reference Ab initio investigations

E-L. Andreici Etimie [a], N.M. Avram [a,e,*], M.G. Brik [b,c,d,e]

[a] Department of Physics, West University of Timisoara, Bd.V. Parvan No. 4, 300223, Timisoara, Romania
[b] School of Optoelectronic Engineering & CQUPT-BUL Innovation Institute, Chongqing University of Posts and Telecommunications, Chongqing, 400065, People's Republic of China
[c] Institute of Physics, University of Tartu, W. Ostwald Str. 1, Tartu, 50411, Estonia
[d] Centre of Excellence for Photoconversion, Vinca Institute of Nuclear Sciences, National Institute of the Republic of Serbia, University of Belgrade, P.O. Box 522, Belgrade, 11001, Serbia
[e] Academy of Romanian Scientists, Ilfov Str. No. 3, 050044, Bucharest, Romania

ARTICLE INFO

Keywords:
Cr^{3+}
Co^{2+}
Spinels
Ab initio calculations
Multi-reference methods

ABSTRACT

The normal spinels (Mg, Zn)Al_2O_4 doped with transition metal (TM) ions Cr^{3+}/Co^{2+} are versatile materials with important electronic, optical and spectral properties. In addition to being used in many applications, they are excellent systems for testing some models and simulation features. The aim of this paper is to present, in the unified frame, the results on d-d transitions and ligand field parameters (LFPs) for the title systems, based on ab initio calculations, combining periodic density functional theory (DFT) supercell approach with ab initio (AI) multi -reference perturbation theory (MRPT) and multi-reference configuration interaction (MRCI) methods. These AI methods, based on complete active space self-consistent-field (CASSCF) reference, allow to calculate and investigate the energy levels of TM ions and the d-d transitions between them. From the AI results the B and C Racah parameters, the spin-orbit coupling (SOC) constant and the LFPs in the frame of the angular overlap model (AOM) were accurately extracted with ab initio ligand field theory (AILFT) protocol, all with subsequent comparison with the experimental data or existing theoretical results in the literature. The calculation technique presented in this paper serves as a predictive formalism for further studies of larger monomer clusters, for which experimental data is unreliable or unavailable.

1. Introduction

The transitional metal (TM) ions, that naturally present in the structures of some crystals or doped as impurity centers (IC) in diamagnetic materials, are responsible for the light absorption and emission; they modify the electronic, magnetic, optical and spectral properties of host materials [1,2]. As such, the doped materials have many applications in chemistry, physics, biology, material science, etc., connected with different technologies like laser technology, nonlinear optics, optical information, phosphor materials, catalysis, etc. [3–7].

The physical reason for modifications of the doped materials' properties is the interaction between the unfilled electron shells of the TM and the field created by the ligands of the host matrices, at the place where the TM is located in crystal. The energy levels of excited state of TM ions in ligand field (LF) and d-d transitions between them, depend on the LFPs. The number of these parameters depends on the local symmetry of the TM ions in the host material and their values depend on complicated interplay of many factors, such as the chemical nature and charges of ligands, covalence of bonds between TM ion and ligands, geometrical characteristics of impurity centers etc. The numerical values of these parameters can be obtained in two different ways. The first way is to use different models and fit experimental data on energy levels, gyromagnetic factors, magnetization values, etc. The second way is based on fundamental laws and equations of physics, capable of getting all needed physical and chemical properties of systems with TM ions. The spectral properties of ion-doped optical materials with TM ions, based on d-d transitions are determined by the energy levels of the TM ions that are a function of LFTs and corresponding wave functions. That is why the knowledge of these parameters and all other properties depending of them, like electronic, optical, spectral, etc. properties, is an

* Corresponding author. Department of Physics, West University of Timisoara, Bd.V. Parvan No. 4, 300223, Timisoara, Romania.
E-mail address: nicolae.avram@e-uvt.ro (N.M. Avram).

https://doi.org/10.1016/j.omx.2022.100188
Received 9 August 2022; Accepted 5 September 2022
Available online 27 September 2022

interesting problem to pursue.

For a TM ion with an unfiled d electron shell, like trivalent chromium ($3d^3$ electronic configuration) or divalent cobalt ($3d^7$ electronic configuration), embedded in a diamagnetic crystal host material, like normal spinels (Mg,Zn)Al_2O_4 crystals, the effective Hamiltonian of the system describes the interaction between open shell electrons of TM with ligand field of the host matrix, the repulsion interactions between d electrons of the TM and the SOC interactions. In the classical LF theory the terms of such Hamiltonian are never computed explicitly but are parametrized and the parameters are adjusted to empirical data.

In the case of lowest site symmetry for the 3d ions, the Hamiltonian depends on 18 parameters: 15 one-electron LF parameters, which describe the interaction of unfilled electron shell with LF of host matrix, two-electron B and C (Racah parameters), describing the Coulomb repulsion between the 3d electrons and SOC constant parameter of TM ion responsible for fine structure of the energy levels of IC. In the classical LFT the number of non-zero parameters of the discussed Hamiltonian can be identified from local symmetry of the impurity ion and treated as the fitting parameters. They are varying until the root mean square (RMS) between experimental and calculated energy levels scheme has minimum value. In the static LFT there are currently numerous models [8] available for the description of the physical and chemical properties of the considered system, the best known being electrostatic model (EM) [9], exchange charge model (ECM) [10], superposition model (SM) [11], angular overlap model (AOM) [12], etc.

The normal spinels $MgAl_2O_4$ and $ZnAl_2O_4$ doped with Cr^{3+}/Co^{2+} were investigated from both experimental [13–15 and reference herein] and theoretical points of view [16–18 and reference herein]; their spectral, optical and electronic properties were modeled in the framework of classical LFT like in the above-mentioned models.

Even if LFPs, obtained by fitting procedure, have clear chemical and physical meanings, in the case of 3d electron, the fitting procedure is limited by the small number of experimental energy levels and the accuracy of their determination. To overcome such difficulty, development of new methods based on computational techniques, is needed. With this aim in view, the ab initio methods and new models, entirely based on fundamental laws and equations of physics, capable to getting all needed physical and chemical properties of systems with TM ions, have been developed. These AI methods are based on the DFT calculations combined with multi-reference (MR) on top of CASSCF [19,20] method, which account for static electron correlation. The results of this method may be improved with MR methods like the N-electron valence second order perturbation theory (NEVPT2) [21,22], the Hermitian Quasi degenerate NEVPT2 (HQD-NEVPT2) [23,24], the second order dynamic correlation dressed complete active space (DCD-CAS2(3)) [25] with dynamic correlations. Many times the spectroscopy-oriented configuration interactions (SORCI) [26], were also used. All the calculations of optical absorption energies using *AI* methods can be done choosing two different options – state averaging (SA), yielding a single set of 3d-MOs shared with all d^n – states and a state specific (SS) option, accounting for orbital relaxations, which vary between different states.

The first aim of this paper is a deep investigations inside of the spectral properties of Cr^{3+}/Co^{2+}: (Mg, Zn)Al_2O_4 systems, in a unified approach, using the AI methods mentioned above, in order to obtain the new information on their energy levels schemes and d-d transition between them. The second one the Ab Initio Ligand Field Theory (AILFT) [27–29] as a powerful link between theory and experiment, allows unambiguously extract all LFPs, SOC constant and Racah parameters B and C) based on multi –reference AI calculations.

The paper is organized as follow: in Section 2 the all relevant details of the Cr^{3+}/Co^{2+}: (Mg, Zn)Al_2O_4 structure and computational methods of investigation of AI embedded cluster model, the multi-reference methods for calculations the energy levels, the d-d transition between them and wave functions will be presented. Section 3 describes all calculated results in relation to the experimental data and interpretation of d-d transitions. Also, the results of simulation of the EPR parameters, g-matrix and the axial zero field splitting D parameter are discussed. The results of the AILFT protocol used to extracted LFPs of TM ions Cr^{3+}/Co^{2+} doped in (Mg, Zn)Al_2O_4 spinels are presented. All obtained results are compared with the experimental data, and associate discussions constitutes the core of the third section. The conclusions and references will close the paper.

2. Computational setup

2.1. Structural DFT studies of hosts

As a starting point, the periodic DFT calculations were performed, focusing on the complete geometry optimization (atomic positions and cell parameters) of pure crystals needed to treat properly the X-ray structural parameters and band gap energy (E_g). The powerful CRYSTAL17 computer code [30] with Gaussian basis sets centered at the atoms was chosen to treat at a quantum mechanical level the bulk crystals. In view of this, several of the most-used functionals, in particular hybrid (B3PW, PBE0, HISS) and exchange-correlation (SVWN, PBESOLXC, SOGGAXC) functionals were tested. It was observed that PBE0 [31] for $MgAl_2O_4$ (magnesium aluminate) and SOGGAXC [32] for $ZnAl_2O_4$ (zinc aluminate) evaluate the experimental data considerably well. In the second step, the main objective was a new full geometry relaxation of the doped systems modeled by the supercell technique. Different type of supercells containing 56 atoms corresponding to a chemical formula $Cr_x(Mg,Zn)(Al_{1-x})_2O_4$ and 112 atoms associated with $Co_x(Mg_{1-x}, Zn_{1-x})Al_2O_4$ chemical complex, were constructed (see Fig. 1.), all related by $x = 0.0625$ (a doping rate of 6.25%).

For our proposed supercells scheme, one of 16 cations of Al^{3+} or Mg^{2+}/Zn^{2+} was isovalent substituted by Cr^{3+} or Co^{2+} impurity ions, therefore no charge compensation is needed. All ions have been described using high quality triple-ζ valence basis-sets with polarization functions (denoted as pob-TZVP-rev2) [33], available via the online library of the CRYSTAL webpage [34]. Other technical details include a Monkhorst–Pack shrinking factor of 8 for reciprocal space sampling, convergence threshold on self-consistent field (SCF) energy for geometry optimization (TOLDEE) as 10^{-7} and a 7 7 7 7 14 (TOLINTEG) value for Coulomb and exchange integral tolerance factors. The crystal structure has been optimized at a stationary point on the potential energy surface by minimizing the total energy with respect to the nuclear coordinates and the lattice parameters. The accuracy for the numerical integration of the DFT potential was controlled by selecting the extra large integration grid (keyword XLGRID) and for accelerating convergence, we chose the Broyden scheme [35]. The percentage of Fock/Kohn-Sham matrices mixing (FMIXING) during the SCF cycle to ensure convergence was set to 30%. Additional effective charges and bond population (PPAN) for both impurity ions and the ligands based on the wave functions were analysed and quantified at the end of the optimization process.

Current DFT methods explored on the geometrical structures mentioned above, to capture the effect of stability that arises from full relaxation of atomic positions and lattice constants, represent the primordial foundation for the next AI treatments.

2.2. Electrostatic embedded cluster model

An accurate AI treatment, starting from optimized doped crystal geometry, automatically involves so-called embedded cluster procedure to simulate periodic boundary conditions of the crystal as close as possible. This embedded cluster procedure is implemented in a computer code ENV, developed by Gellé and Lepetit [36]. Within this approach the entire periodic system is divided into three parts: the inner part representing the quantum cluster (QC), a thick shell covering the cluster known as the boundary region (BR), built from capped effective core potentials (c-ECPs) and the outer part described by a periodic array of point charges (PC). In this context, the role of the c-ECPs is to avoid electron leakage from the bonded O ions at the boundary of the quantum

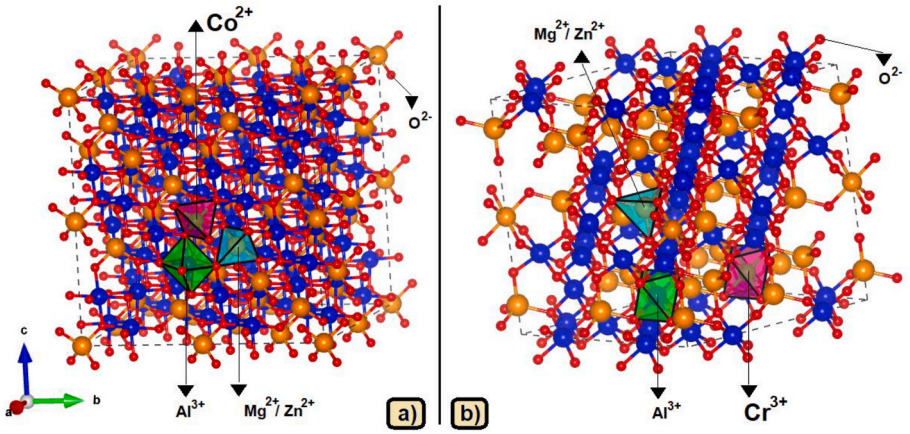

Fig. 1. Equilibrium structure of: (a) 2 × 2 × 2 supercell (112 atoms) of cubic $Fd\bar{3}m$ (Mg,Zn)Al_2O_4 spinel with Co^{2+} ion substituted for Mg^{2+}/Zn^{2+} host ion; (b) 1 × 1 × 1 supercell (56 atoms) of cubic $Fd\bar{3}m$ (Mg,Zn)Al_2O_4 spinel with Cr^{3+} ion substituted for Al^{3+} host ion.

cluster. Central to this procedure is the fulfilling of the charge neutrality condition: qQC + qBR = qPC = 0, a clear need for high-accuracy and well-converged process. Following this strategy, Fig. 2 and Fig. 3 schematically show the $[CoO_4]^{6-}$ and $[CrO_6]^{9-}$ QCs within the periodic electrostatic embedded cluster procedure desiged for our bulk systems.

The visualizing software VESTA [37] was used for illustration of the QC, BR and PC zones corresponding to the embedding scheme described in this work, starting from the ENV files.

2.3. Ab initio electronic structure methods

Quantum chemical calculations were carried out using the ORCA, Version 5 package, based on the new integral engine and task driver SHARK [38–40], testing several MR methods.

The calculations used the relativistic recontracted Karlsruhe basis sets DKH-def2-TZVPP [41] basis set for all atoms alongside with the corresponding auxiliary basis set generated by AutoAux procedure [42] and the second-order scalar relativistic Douglas Kroll Hess (DKH2) [43,44] scalar-relativistic Hamiltonian. For the BR, the c-ECPs for Mg [SD (10,SDF)] [45], Zn [SD(10,MWB)] [46] Al [SD(10,MWB)] and O [SD(2, MWB)] [47] have been obtained from pseudopotential library of the

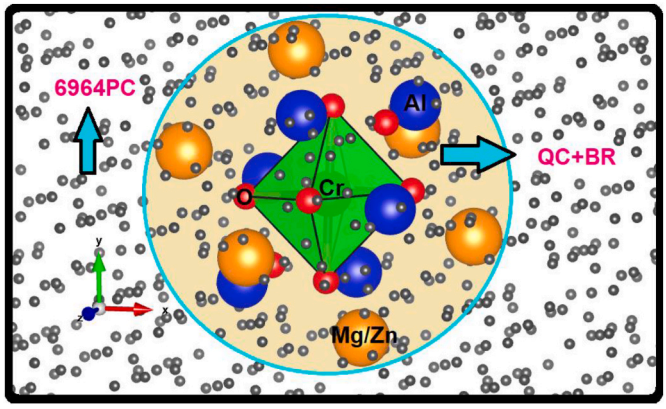

Fig. 3. The schematic construction of a octahedral $[CrO_6]^{9-}$ cluster in (Mg, Zn)Al_2O_4 crystals applying electrostatic embedded cluster scheme.

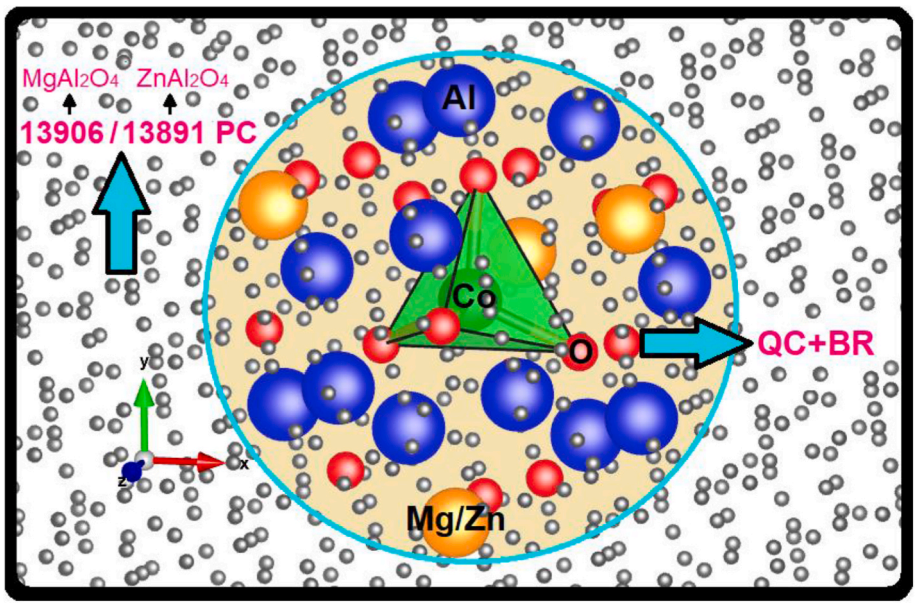

Fig. 2. The schematic construction of a tetrahedral $[CoO_4]^{6-}$ cluster in (Mg, Zn)Al_2O_4 crystals applying electrostatic embedded cluster scheme.

Stuttgart/Cologne group [48]. On the other hand, we have increased the integration grids to seven (SpecialGridIntAcc7) for the metal center in the presence of tight SCF convergence criteria and speeded up the calculations adopting the resolution of identity approximation (RI-JK) [49]. For the SHPs calculations, only SOC was included in the relativistic calculations. The SOC effects were incorporated by quasi-degenerate perturbation theory (QDPT) approach [50], where spin-orbit mean field SOMF(1X) [51] operator accounts for mixing of states with different multiplicities.

The state-averaged complete active space self-consistent field (SA-CASSCF) [19,20] method with three/seven electrons in five d orbitals denoted as CAS (3/7,5) was used to obtain the orbitals for all systems. An initial CASSCF calculation with a smaller active space often provides a good starting point for more sophisticated and much more costly methods, thus reinforcing the idea that is the most frequently used MR method. Although there have been some discussions of using extended active spaces, we stick to a minimal active space for the analysis of these crystals. Averaging was done over all possible roots of all multiplicities, with an equal weight for the quartet and doublet blocks.

Due to the lack of dynamic correlation, CASSCF approach may provide poor zeroth order descriptions and in order to solve this problem, it was deemed necessary to use the most popular post-CASSCF approaches for recovering dynamic correlation called MR methods: MRPT (SC-NEVPT2 [21,22], HQD-NEVPT2 [23,24], DCD-CAS2(3) [25]) and MRCI (SORCI [26]). Among these methods, DCD-CAS2(3) and HQD-NEVPT2 (derived from NEVPT2) belong to the class of multistate multi-reference perturbation theory (MS-MRPT) approaches, which allow for the mixing of multiple electronic CASSCF states under the effect of dynamic correlation. Therefore, multistate dynamic correlation methods do not perform a state-specific correction on top of a single CASSCF state, they construct a Hermitian effective Hamiltonian in a model space, incorporating relaxation effects of complete active space configuration interaction (CASCI) coefficients in order to obtain accurate results. Comparing to DCD-CAS2(3) that used in its construction state-averaged Dyall Hamiltonian, HQD-NEVPT2 method is based on the state-specific zeroth order Hamiltonians that improves the simultaneous description of states with very different physical character and give better results [52]. For difference-dedicated DCD-CAS2(3), we have used a so-called bias correction of the 3rd order to yield reasonable excitation energies for excited states. Note that, at higher level of correlation theory, SORCI is able to restore the proper wave functions even with suboptimal CASSCF orbitals because it is based on the individual selection and difference dedicated correlation interaction (CI) and achieves efficiency through a combination of variation and perturbation theory. The above discussed MR methods are named like this because there are multiple reference determinants contained in the reference wave functions and always start from a CASSCF reference. Beside SA technique, which is the default in ORCA, another feasible computational path to obtain more accurate results is to use SS option, defining a custom weighting scheme for the multiplicity blocks and roots, among desired MR-methods. One should note however that SS orbital optimization (orbitals are optimized for the given state) is challenging to converge and often prone to root-flipping. In our case, we have encountered these convergence problems for some states, but trying different methods for orbital optimizations, was immediately successful only in $[CoO_4]$ cluster. As for the $[CrO_6]$ cluster, to gain all energies of d-d transition states in the SS procedure, a weighting scheme for the multiplicity and root blocks with respect to O_h parent point group symmetries was selected.

2.4. AILFT analysis

AILFT is an exact, non-additive LF tool, used by ORCA software [38–40] in order to obtain an unambiguous one-to-one correspondence between the AI energy levels scheme and that provided by LF models. It can treat two shells electrons at the time, namely first shell, addressed to valence LFT problem involving the d/f electrons and second shell of sp, ds and df valence electrons and core LFT problem including sd, pd, sf and pf electrons. According the AILFT protocol first is performed a simple CASSCF calculations in which the active space consists of n electrons and five orbitals (for $3d^n$ electronic configuration) and taken into account all/several state of a given spin multiplicity of a given TM ion. This approach, originally made for TM ions has been extended to multi-reference configurations, and also to lanthanides [53] and actinides [54] ions. In the last decade the AILFT has been successfully applied to investigate the covalence and magnetic properties, among many others [55 and references herein]. AILFT is a remarkable construction that provides a very powerful link between modern first-principles electronic structure theory and experiment.

Here we present some features of the AILFT protocol, the reader interested in seeing all the possibilities of this protocol can use the original articles [27–29].

For a TM ion with unfiled d electron shell, embedded in a diamagnetic crystal host material, the effective Hamiltonian is given by the equation [56]:

$$\widehat{H}_{LF} = \sum_i \widehat{V}_{LF}(i) + \sum_{i<j} \widehat{G}(i,j) + \xi_{Cr/Co} \sum_i l_i s_i \quad (1)$$

The first terms from eq. (1) describe the interaction between open shell electrons of IC with ligand field of the host matrix, the second one describes the repulsion interactions between 3d electrons of the TM ion, and the last one accounts for spin-orbit interactions. In the classical LF theory the terms of equation (1) are never computed explicitly but they are parametrized and the parameters are adjusted to empirical data.

According to the AILFT protocol for a complex with a 3d ion, based on the AI, CASSCF and its derivative perturbative methods, like SC-NEVPT2, HQD-NEVEPT2, DCD-CAS2(3), etc., is possible to extract ligand-field splitting parameter $\Delta = 10Dq$, low symmetry splitting of the orbital degenerated terms or alternatively, AOM parameters, B and C Racah parameters and SOC constant. For this it is necessary to connect the numerical values of the Hamiltonian matrix elements of equation (1), obtained by AI calculation, with the parameters of a LFT model. Thus, it is possible to compare the calculated one particle or many particle quantities with those ones measured experimental. The AILFT protocol allows also, to recalculate the energy levels scheme with extracted parameters, for different AI methods, and get the root mean square (RMS) values between recalculated values and original ones.

In all used AI methods, the matrix elements of Hamiltonian from eq. (1) were calculated in the basis of five d-orbitals and is obtained all parameters of interest.

So, from diagonalization of V_{LF} matrix from Eq. (1) the energy levels and wave functions of five d_i orbitals are obtained. On the other hand, the 15 independent one-electron parameters of Hamiltonian matrix V_{LF} can be parametrized, for example in the AOM model, by the e_σ parameter (characterizing the metal ion-ligand σ interaction) and the $e_{\pi s}$ and $e_{\pi c}$ parameters (representing in plane and out of plane π type metal ion-ligand interaction), respectively, based on the Eq. (2) [57,58]

$$V_{LF}(a,b) = \sum_{L,\lambda} F_{\lambda a}(\theta_L, \varphi_L, \psi_L) \cdot F_{\lambda b}(\theta_L, \varphi_L, \psi_L) \cdot e_{\lambda,L} \;\; ; \;\; \lambda = \sigma, \pi_s, \pi_c \quad (2)$$

Here L denotes a ligand which has position specified by three polar angles, and $e_{\lambda,L}$ are the AOM corresponding parameters. The least squares fit of 5 × 5 LF matrix, from eq. (2), to AI numerical calculated results, allows to estimate the values for these parameters. In order to get more realistic ligand field parameters - e_σ, and $e_{\pi s} = e_{\pi c} = e_\pi$, Racah B and C parameters and SOC constant for a TM ion doped in a crystal, one needs a direct fit to experimental or computed these parameters using the many particle eigenvalues, from the AOMX software [59]. The interested reader can find examples of scripts for such types of calculations in the paper [60]. Thus, one can obtain deep insight into structure-properties relationships for compounds (real or hypothetical), important information for new molecular and crystal designs, using

AILFT.

We emphasize that parameters set e_σ and e_π of the AOM are not the only ones to interpret the LF matrix resulting from the AILFT procedure. Also the parameters B_{kq} of electrostatic model of CFT [9] can be used for this purpose [9,61].

3. Results and discussions

In this section, we will present and interpret the AI data for the title system originated from the foregoing computational methods and protocol.

3.1. Crystallographic evaluations with respect to the DFT

The spinel oxide crystals (Mg, Zn)Al_2O_4 belong to the cubic space group O_h^7- $Fd\bar{3}m$ (in Schoenflies and Hermann–Mauguin notations), No. 227 in the International Table of Crystallography [62], with eight formula units per unit cell [63,64]. Generally, normal spinels are identified by the AB_2O_4 chemical formula, where Mg^{2+}or Zn^{2+} ions are located at the center of the tetrahedron with $\bar{4}3m$ (T_d) point symmetry (A site), while the Al^{3+} ions are located at the center of the octahedron with $\bar{3}m$ (D_{3d}) symmetry (B site). Every oxygen anion is shared by three octahedra and one tetrahedron. The overall structural appearance of spinel is shown in Fig. 4. The doped metal ions can substitute either A site or B site or both depending upon its valence and site type.

In Table 1, we present the main results of our DFT optimization process, starting from X-Ray data, regarding lattice parameters (a, b, c), distances (d), volumes (Vol) and band gap energy (E_{gap}) using different functionals, as described in Sec 2.1.

As follows from Table 1, PBE0 functional for $MgAl_2O_4$ crystal and SOGGAXC functional for $ZnAl_2O_4$ describe, the band gap energy and volume, with the best average accuracy to the experimental values. It should be kept in mind that an accurate approximation of the band gap energy can be a very good starting choice for describing properties in solid state systems. The good agreement between the calculated and the experimentally measured parameters of pure spinel oxide crystals (Mg, Zn)Al_2O_4 provides a solid foundation for the geometry optimization of doped cases. The optimized structural parameters for the Co^{2+} and Cr^{3+} impurity ions doped in supercells are listed in Table 2, along with interatomic distances and volume changes, as an evaluation tool.

It can be seen that incorporation in (Mg,Zn)Al_2O_4 supercell of Co^{2+} impurity ion decrease the distances and volume while Cr^{3+} impurity ion increase the parameters mentioned above. This situation is consistent with the argument that the ionic radii of the dopant ions are comparable in size than the replaced host ions. Substitution of (Mg/Zn) for the Co^{2+}, in the T_d site symmetry position is accompanied by the compression of the CoO_4 tetrahedron, which is in line with the ionic radii values [67]: Co^{2+}(0.58 Å), Mg^{2+}(0.585 Å) and Zn^{2+}(0.58 Å). The Cr^{3+} doped in the D_{3d} site symmetry position of the Al^{3+} induce an expansion in the supercell and lowers the symmetry of the CrO_6 octahedron. It is also worth mentioning that increasing tendency is expected seeing the ionic radii values [67]: Cr^{3+}(0.615 Å) and Al^{3+}(0.53 Å). Lastly, in order to characterize the nature of bonding of the atomic orbitals for a particular

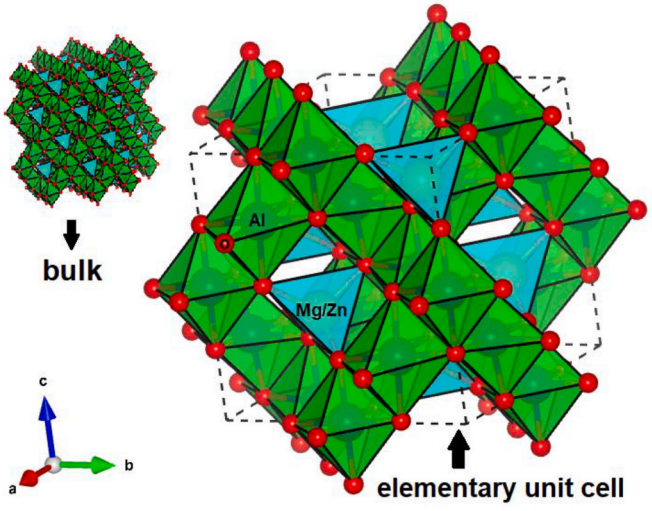

Fig. 4. Elementary unit cell structure of (Mg,Zn)Al_2O_4 with 56 atoms (right view) and perspective (top left) view of the bulk crystal. Drawn with Vesta [37].

Table 1
Summary of experimental and theoretical DFT results of pure $MgAl_2O_4$ and $ZnAl_2O_4$ crystals. Angles $\alpha = \beta = \gamma = 90^\circ$ in all data sets. Percentage differences between experimental and calculated data are given in parenthesis.

$MgAl_2O_4$					
Functional	a = b = c (Å)	d(Mg–O_4) (Å)	d(Al–O_6) (Å)	Vol (Å^3)	E_{gap} (eV)
PBE0	8.0982	1.9480	1.9187	531.083 (0.311%)	7.9867 (2.394%)
B3PW	8.1185	1.9535	1.9233	535.089 (1.068%)	7.4891 (-3.986%)
HISS	8.0623	1.9409	1.9095	524.063 (-1.015%)	8.6560 (10.974%)
Experimental $ZnAl_2O_4$	8.0898[a]	1.9379[a]	1.9209[a]	529.436[a]	7.8[b]
Functional	a = b = c (Å)	d(Zn–O_4) (Å)	d(Al–O_6) (Å)	Vol (Å^3)	E_{gap} (eV)
SOGGAXC	8.0881	1.9457	1.9163	529.110 (0.102%)	4.1175 (8.355%)
PBE0	8.0881	1.9523	1.9130	529.110 (0.102%)	6.8126 (79.279%)
SVWN	8.0150	1.9271	1.8995	514.895 (-2.588%)	4.4365 (16.750%)
Experimental	8.0854[c]	1.9522[c]	1.9120[c]	528.572[c]	3.8[d]

[a] Ref. [63].
[b] Ref. [65].
[c] Ref. [64].
[d] Ref. [66].

Table 2
Structural characteristic of the doped DFT optimized supercells.

Supercell	Impurity ion	Structural parameters (Å)	Impurity-ligand distances (Å) in tetrahedron and octahedron	Volume change[a]
$MgAl_2O_4$ (2 × 2 × 2)	Co^{2+}	a = b = c = 16.1938 (Å) α = β = γ = 90° V = 4246.633 (Å^3)	d(Co–O_4) = 1.9462	−0.047%
$ZnAl_2O_4$ (2 × 2 × 2)		a = b = c = 16.1747 (Å) α = β = γ = 90° V = 4231.611 (Å^3)	d(Co–O_4) = 1.9411	−0.029%
$MgAl_2O_4$ (1 × 1 × 1)	Cr^{3+}	a = b = c = 8.115 (Å) α = β = γ = 89.881° V = 533.709 (Å^3)	d(Cr–$O_{1\text{-}3}$) (Å) = 1.9797 d(Cr–$O_{4\text{-}6}$) (Å) = 1.9798	0.494%
$ZnAl_2O_4$ (1 × 1 × 1)		a = b = c = 8.0988 (Å) α = β = γ = 89.882° V = 531.206 (Å^3)	d(Cr–$O_{1\text{-}3}$) (Å) = 1.9768 d(Cr–$O_{4\text{-}6}$) (Å) = 1.9769	0.396%

[a] The percent changes of doped supercell volume were calculated with respect to that of pure optimized (Mg,Zn)Al_2O_4 crystals.

Table 3
Mulliken population analysis (e−electron units) of pure (Mg,Zn)Al_2O_4 and doped crystals with Co^{2+} or Cr^{3+} impurity ions. Q is Mulliken effective charge and P represents the bond population between atoms. The deviations from formal ionic charges are shown in parentheses.

Atom	Charge Q (e) Bond pop. P (e)	$MgAl_2O_4$	ZnAl2O4
Mg	Q	1.515 (0.485)	–
Zn	Q	–	1.251 (0.749)
Al	Q	1.851 (1.149)	1.711 (1.289)
O	Q	−1.304 (0.696)	−1.168 (0.832)
Co (impurity)	Q	1.301 (0.699)	1.233 (0.767)
Cr (impurity)	Q	1.487 (1.513)	1.371 (1.629)
Mg–O	P	0.062	–
Zn–O	P	–	0.013
Al–O	P	0.139	0.145
Co–O_4	P	−0.002	0.005
Cr–$O_{1\text{-}6}$	P	0.071	0.066

pairs of atoms and the charge distribution in the ternary compounds, such as (Mg,Zn)Al_2O_4 spinel, we employed the Mulliken analysis [68]. Table 3 lists the effective atomic charges and overlap populations of such an analysis mentioned above. Mulliken atomic charges obtained from CRYSTAL 17 [30] calculations reveal non-integer values for all elements, indicating a partial ionic character of pure (Mg,Zn)Al_2O_4 crystals. This deviation of effective Mulliken charges from the formal ionic charges (Mg^{2+},$Zn^{2+}Al^{3+}$,O^{2-}), is large especially in the case of Al ions (see Table 3, column 3, values in parenthesis), revealing that Al–O ions in pure (Mg,Zn)Al_2O_4 crystals are more covalent. It is worthwhile noting that bond population analysis between atoms also reinforce the covalency of Al–O chemical bonding in crystals, whereas Mg–O and Zn–O turn out to be ionic. Concerning the impurities doped in (Mg,Zn)Al_2O_4 crystals, the calculations show a ionic character for Co^{2+}-O_4 pair and a covalent nature of Cr–$O_{1\text{-}6}$ bond. The negative value of Co–O_4 bond population in $MgAl_2O_4$ crystal indicates electronic repulsion.

3.2. Ab initio calculation of the d-d transitions energies

In the Russell-Saunders coupling approximation, the Coulomb interaction among the 3d electrons of the free Cr^{3+} ion, gives rise to the formation of eight distinct spectral terms ^4F, ^4P, ^2G, ^2H, ^2F, $^2D(1,2)$, out of which ^4F is the ground electronic term. By doping Cr^{3+} in (Mg, Zn)Al_2O_4 normal spinels it substitutes for the trivalent aluminum ion in trigonal (D_{3d}) site symmetry [69,70]. The octahedral environment yields a $t_{2g}^3e_g^0$ ground state electronic configuration for Cr^{3+} and splits the five-fold degenerate 3d orbitals into three-fold degenerate t_{2g} orbitals and two-fold degenerate e_g orbitals. In this context, the ground state spectroscopic term ^4F splits into $^4A_{2g}$ (the orbital nondegenerate ground state for three electrons in each of the t_{2g} orbitals) and the $^4T_{2g}$ and $^4T_{1g}$ excited states. Therefore, the three main bands in the absorption spectrum are $^4A_{2g}\rightarrow{}^4T_{2g}$ (^4F), $^4A_{2g}\rightarrow{}^4T_{1g}$ (^4F), associated with the $t_{2g}^3\rightarrow t_{2g}^2e_g^1$ spin-allowed transitionsand $^4A_{2g}\rightarrow{}^4T_{1g}$ (^4P) for the $t_{2g}^3\rightarrow t_{2g}^1e_g^2$ spin allowed transition. These transitions give rise to broad absorption bands and are strongly dependent on the ratio Dq/B of the ligand splitting parameter 10Dq and the Racah B parameter of inter-electronic repulsion. The spin-forbidden transitions from the spin quartet ground state and excited spin doublets give narrow bands with low intensity. The positions of low lying energy levels $^2E(^2G)(t_{2g}^3)$, $^2T_1(^2G)(t_{2g}^3)$ and $^2T_2(^2G)$ (t_{2g}^3) in the Tanabe-Sugano diagram [56] run almost parallel to the $^4A_{2g}$ ground state. Our analysis is based on the case where octahedral symmetry of the Cr^{3+} complex is lowered to trigonal symmetry and each of the spin allowed bands splits into two components. Following the symmetry descent from O_h to D_{3d}, only the orbital triplet states (T) are split into a combination of a doublet (E) and a singlet (A) states, while the orbital singlets and orbital doublets retain their degeneracy and are just displaced. Since the crystal field strength for studied systems is strong (Dq/B > 2.2) [69,70], the first excited state of Cr^{3+} in (Mg, Zn)Al_2O_4 normal spinels is ^2E_g (^2G), which plays an important role in the emission spectra. However, this paper only explores the d-d energy levels from absorption spectrum with remarkable many observed states for spin-forbidden transitions.

The free divalent cobalt ion has a complementary electronic configuration with Cr^{3+} and the same electronic spectral terms. By doping in (Mg, Zn)Al_2O_4 normal spinels it will substitutes the (Mg, Zn) divalent ions without charge compensation, in tetrahedral site symmetry [71]. Unlike the case of Cr^{3+} doped in (Mg, Zn)Al_2O_4 crystals in case of doping of the Co^{2+} ion, in the same crystals, the crystal field is low (Dq/B < 0.5) and therefore the first excited state of the divalent cobalt ion is a quartet state ($^4T_2$), which comes from the splitting of the fundamental term ^4F of cobalt located in the tetrahedral field of the host matrices. For both cases of Cr^{3+} and Co^{2+} doped (Mg, Zn)Al_2O_4 crystals the experimental data on the energies of the excited levels as well as on the d-d transitions between them [69–71] are insufficient or even scarce. Moreover, the existence and nature of experimental peaks are uncertain or they cannot be observed experimentally. Under these conditions, the AI investigation of the d-d transitions in the case of systems Cr^{3+}/Co^{2+}: (Mg, Zn)Al_2O_4, using multi-reference methods, is required not only to understand d−d transitions in such monomeric clusters but they come to complete the experimental data, the theoretical results existing in the specialized literature, as well as that obtained by us for other systems [60,72–74].

In order to choose the best method consistent with the experimental results, two arguments were taken into account in this work, namely the energy levels ordering and Root Mean Square (RMS) errors of computed vs experimental d-d transitions. For the sake of brevity, we are focused only on energy levels and d-d transitions that are relevant for the interpretation of d-d transitions in the studied spectral range, namely that from $^4A_2$ ground state of both transition ions to first excited states $^4T_2(F)$, $^4T_1(F)$, $^4T_1(P)$ (quartet states) and $^2E(^2G)$, $^2T_1(^2G)$, $^2T_2(^2G)$, $^2A_1(^2G)$, doublet states, respectively. First shell involving d valence electrons and minimal complete active space CAS(3,5), containing 3 electron and five orbitals for trivalent chromium ion, and CAS (7,5) for divalent cobalt, respectively, is a good strategy for the 3d electron configurations with incomplete valence 3d shell, due to their strongly localized orbitals. Starting from the minimal active space CAS (3,5), SC-NEVPT2, HQD-NEVPT2, DCD-CAS2(3) and SORCI calculations are performed on top of the converged CASSCF wave functions in the framework of SA and SS methods. The results of AI computation with

Table 4
AI energy (cm^{-1}) for Cr^{3+}: (Mg,Zn)Al_2O_4.

Energy levels		Exp [69, 70].	Cr^{3+}:$MgAl_2O_4$		Exp [69].	Cr^{3+}:$ZnAl_2O_4$	
O_h	D_3		DCD-CAS2 (3) (3,5) SA	DCD-CAS2 (3) (3,5) SS		DCD-CAS2 (3) (3,5) SA	DCD-CAS2 (3) (3,5) SS
$^4A_{2g}(^4F)$	$^4A_2$	**0**	0	0	**0**	0	0
$^2E_g(^2G)$	^2E	**14656**	16454	16237	**14575**	16496	16317
$^2T_{1g}(^2G)$	^2E	**14801**	17235	16847	**}**	17237	16877
{	$^2A_2$	**15069**	17856	17485	**15166**[a]	17836	17489
$^4T_{2g}(^4F)$	^4E	**}18500**	19289	20048	**}18756**	19427	20210
{	$^4A_1$		19755	20526		19618	20414
$^2T_{2g}(^2G)$	$^2A_1$	**}22100**	23628	22719	**}23974**	23789	22925
{	^2E		25353	24484		25364	24546
$^4T_{1g}(^4F)$	$^4A_2$	**}25200**	25917	26278	**}25832**	25928	26318
{	^4E		27711	28089		27785	28188
$^2A_{1g}(^2G)$	$^2A_1$	**30865**[a]	33029	32469	**30920**[a]	33110	32597
$^4T_{1g}(^4P)$	^4E	**}**	41701	41462	**}**	42032	41846
{	$^4A_2$	**40600**[a]	44883	44610	**40860**[a]	44495	44281
RMS errors (cm^{-1})			**2050**	**1874**	**RMS errors (cm^{-1})**	**1602**	**1548**

[a] Calculated from Sugano-Tanabe diagram.

DCD-CAS2(3) method, with both SA and SS procedures, having minimum RMS errors, for Cr^{3+}: (Mg, Zn)Al_2O_4, are given in Table 4. The same type of results were obtained for Co^{2+}(Mg, Zn)Al_2O_4 with SORCI method for SA and SC-NEVPT2 method in SS procedure, are putted in Table 5.

For all other AI methods, the results are given in Tables S1–S4, respectively of SI material.

The calculations result from these tables provide useful and interesting information regarding the vertical d-d transitions energies for studied systems. First of all, we underline that MR calculations give much higher d−d transition energies compared to the experimental assignments and this is a general characteristic of AI methods used [7–9]. AI CASSCF method used in our computations, accounts for static electron correlations, and its wave's functions is taken as zero-order functions for a more rigorous calculations based on the other AI methods which take into account the dynamic electron correlations. Unfortunately, the results of d-d transition energies obtained with this method (Tables S1–S4) have the highest value of RMS errors and, also the wrong ordering of state with different spins. For example, in the case of Cr^{3+}/Co^{2+}: (Mg, Zn)Al_2O_4 systems the computed energies of the states $^2E_g(^2G)$ and $^2T_{1g}(^2G)$ have higher energies than $^4T_{2g}(^4F)$ excited state. In all other AI method of calculations, the correct ordering of the states is reproduced, even if the d-d transition energies exceed the experimental data with ~ 1000–2000 cm^{-1}.

The best results regarding the energies of d-d transitions can be obtained with the ab initio multi-reference methods, using the state specific procedure obtained by DCD-CAS2(3) for Cr^{3+}(Mg, Zn)Al_2O_4-Table 4 and SC-NEVPT2 for Co^{2+}:(Mg, Zn)Al_2O_4 –Table 5. These procedures provide both the correct order of energy levels and their values, which are both close to the experimental data.

3.3. Spin-Hamiltonian parameters

For a paramagnetic system the spin-Hamiltonian is given by [56].

$$\widehat{H}_{spin} = \widehat{H}_{Ze} + \widehat{H}_{ZFS} = \beta \boldsymbol{B}\boldsymbol{g}\widehat{S} + \widehat{S}\boldsymbol{D}\widehat{S} \quad (3)$$

where the notations are the well known [56]. The 3 × 3 **g** and **D** matrices, which describe the electronic Zeeman and zero-field splitting (ZFS) of the ground state, respectively and are calculated with the AI multi-reference methods, were used in this paper. The form of **g** and **D** matrices depends on the site symmetry of the paramagnetic ion and on the axes of the system of reference. In the case of Co^{2+} doped (Mg, Zn)Al_2O_4 the gyromagnetic factors $g_x = g_y = g_z$ due the tetrahedral site symmetry in both host matrix. For Cr^{3+} doped in (Mg, Zn)Al_2O_4 systems, with D_{3d} site symmetry and z axes of Cartesian reference system along the (111) cubic axes of the crystal, the equation (3) has the form [56].

$$H_{spin} = D\left[\widehat{S}_z^2 - (1/3)S(S+1)\right] + g_{\perp}\left(B_x\widehat{S}_x + B_y\widehat{S}_y\right) + g_{\parallel}B_z\widehat{S}_z \quad (4)$$

The results of AI calculations the spin-Hamiltonian parameters are collected in Table 6.

As seen from Table 6, the closest results with measured data for Co^{2+}: (Mg, Zn)Al_2O_4 are obtained for SC-NEVPT2 and HQD-NEVPT2 methods in the case of g factors, whereas for Cr^{3+}:(Mg, Zn)Al_2O_4 the best calculated values was obtained with SORCI method for axial D parameter and best value for g factors were derived also for SC-NEVPT2 and HQD-NEVPT2 methods, like in case of Co^{2+}:(Mg, Zn)Al_2O_4.

3.4. AILFT

MR-type AI methods allow the calculation of the energy levels of the transition metal ions doped in the crystals and corresponding eigenvalues of the full many-particle Hamiltonian, as well as the d-d transitions between energy levels. Moreover, these methods also allow the extraction, using the AILFT protocol and ORCA 5.03 software, the LFPs parameters, from the Hamiltonian (1) in one-electron model. For this it is necessary to calculate the matrix elements of the LFT matrices of terms from Hamiltonian (1), in the base of five orbitals d_{xy}, d_{yz}, d_z^2, d_{xz} and $d_{x^2-y^2}$ of 1 d electron. For example, for Cr^{3+} impurity ion in $ZnAl_2O_4$ the 5 × 5 V_{LF}(DCD-CAS2(3)) matrix of first term from Eq. (1), with minimal CAS (3,5), has the form

$$\begin{pmatrix} d_{xy} & d_{yz} & d_z^2 & d_{xz} & d_{x^2y^2} \\ d_{xy}\ -1.873409 & 0.003182 & 0.003178 & -0.000012 & -0.006035 \\ 0.003182 & -1.958549 & 0.000434 & 0.005123 & 0.000391 \\ 0.0031178 & 0.000434 & -1.958550 & -0.005128 & 0.000411 \\ -0.000012 & 0.005123 & -0.005128 & -1.873362 & -0.000176 \\ -0.0060135 & 0.000391 & 0.000411 & -0.000176 & -1.958544 \end{pmatrix} \quad (5)$$

By diagonalization this matrix the AILFT orbital energies (cm^{-1}) are obtained: 0 (a_1), 410.3 ($e_{(1)}$) and 19059.4 ($e_{(2)}$). This means that in the strong crystal field approach, the fivefold degenerated ^2D ground state of a d electron, will be split in octahedral crystal field of $ZnAl_2O_4$ host matrix, in two degenerate energy levels e_g and t_{2g}. By doping the gahnite crystal with Cr^{3+} the site symmetry of trivalent chromium ion decreases to trigonal one, and the threefold degenerated energy levels t_{2g} will split, additionally due trigonal field, into two sublevels, one nondegenerate energy level (a), with energy 410.3 cm-1 and another one, double degenerated (e1), with zero value of energy. The double degenerate energy level (e2), with 19059.4 cm^{-1} energy, don't split. In Fig. 5 the 3d-orbital energies and shapes from AILFT calculations with DCD-CAS2 (3), CAS(3, 5) for Cr^{3+}:$ZnAl_2O_4$ are illustrated.

From the splitting terms of Fig. 5 the ligand field parameter 10Dq = 18923 cm^{-1} is calculated, and from matrix elements of the second term of Eq (1), the Racah parameters B = 808.6 cm^{-1} and C = 3409.4 cm^{-1} are extracted. The spin-orbit coupling constant ξ = 254.82 cm^{-1} is extracted from last term of the Hamiltonian (1). For the.

Table 5
AI energy levels (cm^{-1}) for Co^{2+}: (Mg, Zn)Al_2O_4.

Energy levels (Td notations)	Co^{2+}: $MgAl_2O_4$			Energy levels (Td notations)	Co^{2+}: $ZnAl_2O_4$		
	Exp [13].	SORCI (7,5) SA	SC-NEVPT2 (7,5) SS		Exp [71].	SORCI (7,5) SA	SC-NEVPT2(7,5) SS
$^4A_2(^4F)$	0	0	0	$^4A_2(^4F)$	0	0	0
$^4T_2(^4F)$	4200	3936	4494	$^4T_2(^4F)$	4138	3973	4540
$^4T_1(^4F)$	7300	6967	7654	$^4T_1(^4F)$	7396	7110	7729
$^2E(^2G)$	14893	17154	17354	$^2E(^2G)$	15732	17301	17346
$^2T_1(^2G)$	15750	17465	17382	$^2T_1(^2G)$	16113	17568	17366
$^4T_1(^4P)$	17200	17574	18618	$^4T_1(^4P)$	16410	17619	18654
$^2A_1(^2G)$	–	19392	19031	$^2A_1(^2G)$	18250	19367	19051
$^2T_2(^2G)$	18140	20493	20772	$^2T_2(^2G)$	18860	20510	20805
$^2T_2(^2P)$	20940	22494	22800	$^2T_1(^2P)$	21020	22485	22816
$^2T_1(^2P)$	21370	22875	22896	$^2T_2(^2P)$	22100	22992	22899
RMS errors (cm^{-1}) →		**1453**	**1645**	**RMS errors (cm^{-1}) →**		**1170**	**1406**

Table 6
SHPs (g-factors and ZFS parameter D (in cm^{-1})) calculated with different SA methods for minimal active space.

SHPs	Crystals	Expt.	CASSCF (3,5)	SC-NEVPT2(3,5)	HQD-NEVPT2 (3,5)	DCD-CAS2(3) (3,5)	SORCI(3,5)
$g_x = g_y = g_z = g$	Co^{2+}:$MgAl_2O_4$	2.25[a,b]	2.4556	2.2572	2.2569	–	2.2934
$g_x = g_y = g_z = g$	Co^{2+}:$ZnAl_2O_4$	2.22[c]	2.3085	2.2562	2.2558	–	2.2907
$g_z = g_{\|}$	Cr^{3+}:$MgAl_2O_4$	1.985[d]	1.9722	1.9768	1.9769	–	1.9804
$g_x = g_y = g_{\perp}$		1.983[d]	1.9652	1.9710	1.9710	–	1.9756
g_{iso}		1.9836	1.9676	1.9729	1.9730	–	1.9772
D		0.915[d]	1.0121	1.0296	1.0500	1.0621	1.0851
$g_z = g_{\|}$	Cr^{3+}:$ZnAl_2O_4$	1.9840[e]	1.9715	1.9761	1.9762	–	1.9797
$g_x = g_y = g_{\perp}$		1.9798[e]	1.9656	1.9713	1.9713	–	1.9760
g_{iso}		1.9812[e]	1.9676	1.9729	1.9729	–	1.9772
D		0.9304[e]	0.9007	0.9155	0.9336	0.9430	1.0374

[a] [75].
[b] [76].
[c] [64].
[d] [69].
[e] [77].

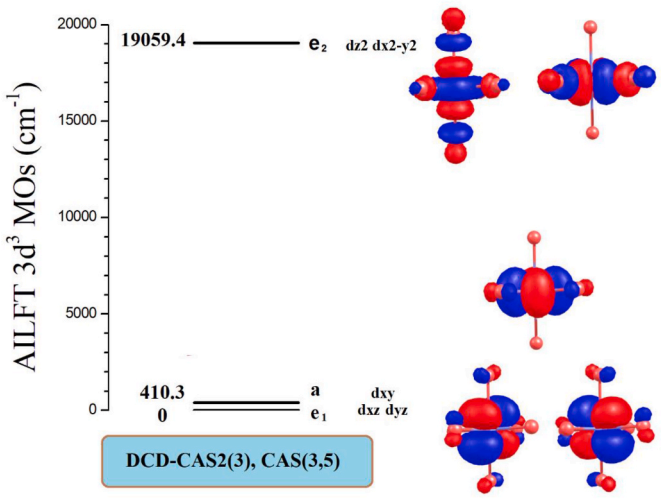

Fig. 5. Energies and shapes of molecular orbitals of Cr^{3+}:$ZnAl_2O_4$. AILFT calculations with DCD-CAS2(3), CAS(3,5) and plotted with Chemcraft [78]. Contour value of 0.030 electron/$Bohr^3$.

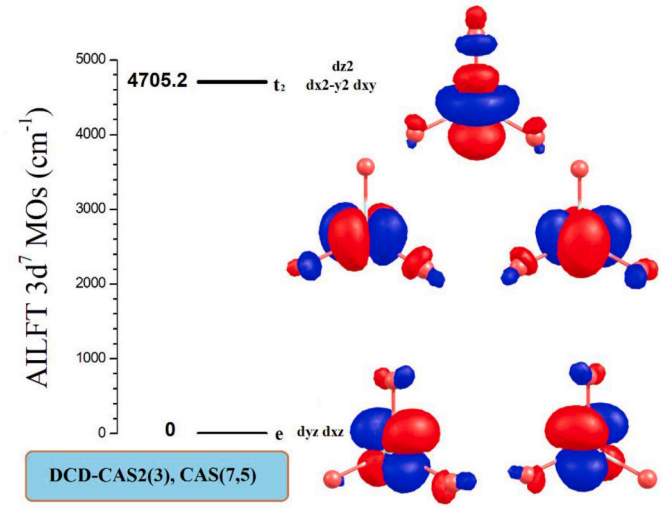

Fig. 6. Energies and shapes of molecular orbitals of Co^{2+}:$ZnAl_2O_4$. AILFT calculations with DCD-CAS2(3), CAS(7,5) and plotted with Chemcraft [78]. Contour value of 0.030 electron/$Bohr^3$.

Co^{2+}:$ZnAl_2O_4$ the AILFT calculations, with DCD-CAS2(3), CAS(7,5) give the results presented in Fig. 6.

In this case the AILFT protocol gives 10Dq = 4705.2 cm^{-1}, B = 938.9 cm^{-1}, C = 3880.4 cm^{-1} and SOC ξ = 510.5 cm^{-1}.

Like in above cases the results of the AILFT calculations allows to obtain the splitting LFPs, the extractions the Racah parameters B and C and the SOC for Cr^{3+}/Co^{2+} doped in (Mg, Zn) Al_2O_4. These results are available in the Table S5 of SI.

The AILFT protocol allows not only the extraction of LFPs, using AI calculations, but also the obtaining the parameters that characterize the classical models used in the semi empirical LFT, such as AOM [12], a popular model among chemists. This model uses two parameters e_σ and e_π to characterize the σ and π interactions of the Cr^{3+}/Co^{2+} impurity ions with the O^{2-} ligands from the first coordination sphere. The two parameters e_σ and e_π depend only on the distance between the impurity ion and the corresponding ligand [79].

There are two methods for numerical calculation of the e_σ and e_π parameters of AOM. The first method is based on the least squares fit of the matrix elements of the equation (2) with the numerical values from the matrix (3), calculated with ab initio methods. The second method of extraction the AOM parameters consists in a direct fit to energies (experimentally deduced or AI computed) d-d transitions using the AOMX software [59]. Simultaneously with the calculation of the e_σ and e_π parameters of AOM, can also be fitted B and C Racah parameters and SOC constant, based on same multi-reference AI calculations. Using the e_σ and e_π parameters the splitting parameter Δ (O_h) = 10 Dq (O_h) of octahedral field and.

Δ (T_d) = 10Dq (T_d) splitting parameter of tetrahedral field are calculated with equation (4) and, respectively (5) [79].

$$\Delta (O_h) = 3\, e_\sigma - 4\, e_\pi \quad (4)$$

$$\Delta (T_d) = -4\, e_\sigma/3 + 16\, e_\pi/9 \quad (5)$$

Finally, neglecting SOC interaction, the LFPs (cm^{-1}) for Cr^{3+}/Co^{2+}: (Mg, Zn)Al_2O_4 named crystal field splitting parameter Δ (O_h)/Δ (T_d), AOM e_σ and e_π, and Racah B and C parameters, computed for experimental data, DCD-CAS2(3), SORCI MR and SC-NEVPT2 methods are collected in Table 7.

From this Table it seen that although the e_σ and e_π parameters vary within quite wide limits, the splitting LFP parameter is approximately the same for Cr^{3+} and respectively Co^{2+}, independent of the AI used method.

The LFPs from Table 7, extracted using the AILFT protocol, can be used to recalculate the energy levels of Cr^{3+} and Co^{2+} ions doped in the (Mg, Zn) Al_2O_4 spinel to study the d-d transitions between them and to calculate the RMS errors between the recalculated and the initial values.

Table 7
LFPs for Cr^{3+}/Co^{2+}: (Mg, Zn)Al_2O_4. All parameters are in cm^{-1}.

Crystal	Methods		B	C	e_σ	e_π	Δ^*/Δ^{**}	RMS
Cr^{3+}: $MgAl_2O_4$	Experimental [69,70]		685	3175	6630	156	19266	300
	SA	DCD-CAS2(3)	791	3566	6936	178	20096	107
	SS	DCD-CAS2(3)	766	3439	7022	195	20286	424
Cr^{3+}:$ZnAl_2O_4$	Experimental [69]		516	3572	7226	466	19814	107
	SA	DCD-CAS2(3)	786	3590	6731	17	20125	148
	SS	DCD-CAS2(3)	761	3434	7015	181	20321	503
Co^{2+}:$MgAl_2O_4$	Experimental [13]		802	3247	3801	480	−4215	282
	SA	SORCI	831	4014	3693	502	−4032	146
	SS	SC-NEVPT2	869	3877	3966	499	−4401	249
Co^{2+}:$ZnAl_2O_4$	Experimental [71]		743	3709	3755	743	−3686	319
	SA	SORCI	829	4020	3758	516	−4094	155
	SS	SC-NEVPT2	868	3874	3999	499	−4445	254

$\Delta^* = \Delta\ (O_h) = 3\ e_\sigma\text{-}4\ e_\pi$; $\Delta^{**} = \Delta\ (T_d) = -4\ e_\sigma/3 + 16\ e_\pi/9$.

4. Conclusions

In this paper we theoretically investigated, by ab inito route, the d-d transition for trivalent chromium and respectively divalent cobalt doped in normal spinels (Mg, Zn) Al2O4. We combined the DFT periodic calculations of Crystal 17 software for all geometry optimization and have generated an embedded cluster for impurity ions according Gelle-Lepetit procedure. All energy levels calculations and d-d transitions between them were made with the Orca 5.03 computer program, and were based on ab initio MR (MRPT and MRCI) methods, with minimum CAS (3,5) for Cr^{3+} and CAS (7,5) for Co^{2+} respectively. For Cr^{3+}:(Mg, Zn)Al_2O_4 the minimum RMS were obtained for DCD-CAS2(3) method (SA and SS procedures), while for Co^{2+}:(Mg, Zn)Al_2O_4 system the SORCI method (for SA procedure) and SC-NEVPT2 method (for SS procedure), gibe the best results. For these states we extracted the LFPs with AILFT protocol and also computed the AOM parameters. The energies levels and d-d transitions between them were recalculated with these parameters and the results present small value for RMS errors. Besides, the LFTs parameters we calculated also the SH parameters for cases of interest. All results are discussed, compare between them and with experimental data and information presented are robust and reliable. Some of them are suggested for experimental testing. The models, methods and protocol from this paper can serve not only to understand the d−d transitions in monomeric clusters but also as a predictive tool for further studies of larger monomer clusters for which experimental data are unreliable or unavailable. Such investigations are ongoing.

CRediT authorship contribution statement

E.-L. Andreici Eftimie: Methodology, ab initio calculations, Data analysis and discussion, Writing – review & editing; N. M. Avram: Conceptualization, Methodology, ab initio ligand field theory calculations, Data Formal analysis and discussion, Writing – review & editing; M. G. Brik: Methodology, Data analysis and discussion, Writing – review & editing. All authors have read and agreed to the published version of the manuscript.

Declaration of competing interest

The authors declare that they have no known competing financial interests or personal relationships that could have appeared to influence the work reported in this paper.

Acknowledgments

N.M.A. appreciates the supports from the West University of Timisoara (Grant Nr. 67509/25/24.09.2021) and thank Professor Mihail Atanasov for providing the AOMX computer program.

M.G.B. appreciates the supports from the Program for the Foreign Experts (Grant No. W2017011) offered by Chongqing University of Posts and Telecommunications and the National Foreign Experts Program for "Belt and Road Initiative" Innovative Talent Exchange (Grant No. DL2021035001L), Estonian Research Council grant PUT PRG111, European Regional Development Fund (TK141), andNCN project 2018/31/B/ST4/00924.

Appendix A. Supplementary data

Supplementary data to this article can be found online at https://doi.org/10.1016/j.omx.2022.100188.

References

[1] M.G. Brik, C.-G. Ma, Theoretical Spectroscopy of Transition Metal and Rare Earth Ions: from Free State to Crystal Field, Jenny Stanford Publishing, Singapore, 2020.
[2] N.M. Avram, M.G. Brik (Eds.), Optical Properties of 3d-Ions in Crystals: Spectroscopy and Crystal Field Analysis, Springer and Tsinghua University Press, 2013.
[3] C.A. Morrison, Crystal Fields for Transition-Metal Ions in Laser Host Materials, Springer-Verlag, Berlin, 1992.
[4] B. Henderson, R.H. Bartram, Crystal-Field Engineering of Solid-State Laser Material, Cambridge University Press, 2000.
[5] R.-S. Liu (Ed.), Phosphors, up Conversion Nano Particles, Quantum Dots and Their Applications, Springer -Verlag, 2017.
[6] H. Aizawa, H. Uchiyama, T. Katsumata, S. Komuro, T. Morikawa, H. Ishizawa, E. Toba, Meas. Sci. Technol. 15 (2004) 1484–1489.
[7] K. Sharma, D. Gourier, B. Viana, T. Maldiney, E. Teston, D. Scherman, C. Richard, Opt. Mater. 36 (2014) 1901–1906.
[8] P. Su, C.-G. Ma, M.G. Brik, A.M. Srivastava, Opt. Mater. 78 (2018) 129–136.
[9] M.T. Hutchings, Solid State Phys. 16 (1964) 227–273.
[10] B.Z. Malkin, A.A. Kaplyanskii, B.M. Macfarlane (Eds.), Spectroscopy of Solids Containing Rare-Earth Ions, North-Holland, Amsterdam, 1987.
[11] D.J. Newman, Adv. Phys. 20 (1971) 197–256.
[12] C.E. Schäffer, C.K. Jørgensen, Mol. Phys. 9 (1965) 401–412.
[13] P.J. Deren, W. Strek, U. Qetliker, H.U. Gudel, Phys. stat. sol. 182 (1994) 241–251.
[14] N.V. Kuleshov, V.P. Mikhailov, V.G. Scherbitsky, B.I. Minkov, T.J. Glynn, R. Scherloc, J. Lumin. 55 (1993) 265–269.
[15] K. Izumi, S. Miyazaki, S. Yoshida, T. Mizokawa, E. Hanamura, Phys. Rev. B 76 (2007), 075111.
[16] J.M. Garcia-Lastra, M.T. Barriuso, J.A. Aramburu, Phys. Rev. B 78 (2010), 085117.
[17] H. Wang, X.Y. Kuang, A.J. Mao, X. Yang, Chem. Phys. Lett. 436 (2007) 194–198.
[18] M.G. Brik, J. Papan, D.J. Jovanovic, M.D. Dramicanin, J. Lumin. 177 (2016) 145–151.
[19] B.O. Roos, P.R. Taylor, P.E.M. Sigbahn, Chem. Phys. 48 (2) (1980) 157–173.
[20] P. Siegbahn, A. Heiberg, B. Roos, B. Levy, Phys. Scripta 21 (1980) 323.
[21] C. Angeli, R. Cimiraglia, S. Evangelisti, T. Leininger, J.-P. Malrieu, J. Chem. Phys. 114 (2001), 10252.
[22] C. Angeli, R. Cimiraglia, J.-P. Malrieu, Chem. Phys. Lett. 350 (2001) 297.
[23] L. Lang, K. Sivalingam, F. Neese, J. Chem. Phys. 152 (2020), 014109.
[24] C. Angeli, S. Borini, M. Cestari, R. Cimiraglia, J. Chem. Phys. 121 (2004) 4043.
[25] S. Pathak, L. Lang, F. Neese, J. Chem. Phys. 147 (2017), 234109.
[26] F. Neese, J. Chem. Phys. 119 (18) (2003) 9428.
[27] M. Atanasov, D. Ganyushin, K. Sivalingam, F. Neese, Struct. Bond 143 (2012) 149–220.
[28] S.K. Singh, J. Eng, M. Atanasov, F. Neese, Coord. Chem. Rev. 433 (2017) 2–25.
[29] L. Lang, M. Atanasov, F. Neese, J. Phys. Chem. A 124 (2020) 1025–1037.
[30] R. Dovesi, A. Erba, R. Orlando, C.M. Zicovich-Wilson, B. Civalleri, L. Maschio, M. Rerat, S. Casassa, J. Baima, S. Salustro, B. Kirtman, WIREs Comput Mol Sci 8 (2018), e1360.
[31] C. Adamo, V. Barone, J. Chem. Phys. 110 (1999) 6158–6170.
[32] Y. Zhao, D.G. Truhlar, J. Chem. Phys. 128 (2008), 184109.

[33] D. Vilela Oliveira, M.F. Peintinger, J. Laun, T. Bredow, J. Comput. Chem. 40 (2019) 2364–2376.
[34] 2022-31-05, https://www.crystal.unito.it/basis-sets.php.
[35] C.G. Broyden, Math. Comput. 19 (1965) 577.
[36] A. Gellé, M.-B. Lepetit, J. Chem. Phys. 128 (24) (2008), 244716.
[37] K. Momma, F. Izumi, J. Appl. Crystallogr. 41 (2008) 1272.
[38] F. Neese, Wiley Interdiscip. Rev. Comput. Mol. Sci. 2 (2012) 73–78.
[39] F. Neese, Wiley Interdiscip. Rev. Comput. Mol. Sci. 8 (2018) 4–9.
[40] F. Neese, Wiley Interdiscip. Rev. Comput. Mol. Sci. e1606 (2022) 1–15, https://doi.org/10.1002/wcms.1606.
[41] D.A. Pantazis, X.-Y. Chen, C.R. Landis, F. Neese, J. Chem. Theor. Comput. 4 (2008) 908–919. Weigend, R. Ahlrichs, Phys. Chem. Chem. Phys. 7, (2005) 3297.
[42] G.L. Stoychev, A.A. Auer, F. Neese, J. Chem. Theor. Comput. 13 (2) (2017) 554–562.
[43] B.A. Hess, Phys. Rev. A 33 (1986) 3742.
[44] G. Jansen, B.A. Hess, Phys. Rev. A 39 (1989) 6016.
[45] P. Fuentealba, L.v. Szentpaly, H. Preuss, H. Stoll, J. Physiol. Biochem. 18 (1985) 1287.
[46] M. Dolg, U. Wedig, H. Stoll, H. Preuss, J. Chem. Phys. 86 (1987) 866.
[47] A. Bergner, M. Dolg, W. Kuechle, H. Stoll, H. Preuss, Mol. Phys. 80 (1993) 1431.
[48] 2022-23-06, http://www.theochem.uni-stuttgart.de/pseudopotentials/.
[49] F. Neese, J. Chem. Theor. Comput. 24 (2003) 1740–1747.
[50] D. Ganyushin, F. Neese, J. Chem. Phys. 125 (2006), 024103.
[51] F. Neese, J. Chem. Phys. 122 (2005), 034107.
[52] L. Lang, Phd Thesis, Bonn University, December 2019.
[53] D. Aravena, M. Atanasov, F. Neese, Inorg. Chem. 55 (2016) 4457–4469.
[54] J. Jung, M. Atanasov, F. Neese, Inorg. Chem. 56 (2017) 8802–8816.
[55] M. Atanasov, D. Aravena, E. Saturina, E. Bill, D. Maganas, F. Neese, Coord. Chem. Rev. 289–290 (2015) 177–214.
[56] S. Sugano, Y. Tanabe, H. Kamimura, Multiplets of Transition-Metal Ions in Crystals, Academic Press, New York, 1970.
[57] C.E. Schäffer, Struc. Bond. 51 (1968) 68–95.
[58] V.G. Chilkuri, S. DeBeer, F. Neese, Inorg. Chem. 56 (2017) 10418–10436.
[59] H. Adamsky, T. Schönherr, M. Atanasov, in: A.B.P. Lever (Ed.), Comprehensive Coordination Chemistry II, vol. 2, Elsevier, Amsterdam, 2003.
[60] M. Atanasov, E.-L. Andreici Eftimie, N.M. Avram, M.G. Brik, F. Neese, Inorg. Chem. 61 (2022) 178–192.
[61] D.J. Newman, G.K.C. Ng, Crystal Field Handbook, Cambridge University Press, Cambridge, 2000.
[62] T. Hahn, International Table for Crystallography, A, Springer, 2005.
[63] L.W. Finger, R.M. Hazen, A.M. Hofmeister, Phys. Chem. Miner. 13 (1986) 215–220.
[64] J. Popovic, E. Tkalcec, B. Grzeta, S. Kurajica, B. Rakvin, Am. Mineral. 94 (2009) 771–776.
[65] M.L. Bortz, R.H. French, D.J. Jones, R.V. Kasowski, F.S. Ohuchi, Phys. Scripta 41 (1990) 537–541.
[66] S.K. Sampath, J.F. Cordaro, J. Am. Ceram. Soc. 81 (1998) 649.
[67] St Hugh, C. O'Neill, A. Vrotsky, Am. Mineral. 68 (1983) 181–194.
[68] R.S. Mulliken, J. Chem. Phys. 23 (1955) 1833–1840.
[69] D.L. Wood, G.F. Imbusch, R.M. Macfarlane, P. Kisliuk, D.M. Larkin, J. Chem. Phys. 48 (11) (1968) 5255–5263.
[70] B.K. Sevast'yanov, Crystallogr. Rep. 48 (2003) 989–1041.
[71] J. Ferguson, D.L. Wood, L.G. van Uitert, J. Chem. Phys. 51 (1969) 2904–2910.
[72] E.-L. Andreici Eftimie, C.N. Avram, M.G. Brik, N.M. Avram, J. Phys. Chem. Solid. 113 (2018) 194–200.
[73] E.-L. Andreici Eftimie, C.N. Avram, M.G. Brik, V.A. Chernyshev, N.M. Avram, J. Lumin. 214 (2019), 0116577.
[74] E.-L. Andreici Eftimie, N.M. Avram, Phys. Scripta 95 (2020), 044005.
[75] A. Abragam, B. Bleaney, Electron Paramagnetic Resonance of Transition Ions, Clarendon press, Oxford, 1970.
[76] M. Iakovleva, E. Vavilova, H.-J. Grafe, S. Zimmermann, A. Alfonsov, H. Luetkens, H.-H. Klauss, A. Maljuk, S. Wurmehl, B. Büchner, V. Kataev, Phys. Rev. B 91 (2015), 144419.
[77] P. Schindler, P. Gerber, F. Waldner, Helv. Phys. Acta 43 (1970) 583–592.
[78] G.A. Zhurko, D.A. Zhurko, ChemCraft, version 1.8, html: www.chemcraftprog.com, 2022-23-07.
[79] M. Gerloch, R.C. Slade, Ligand-field Parameters, Cambridge University Press, 1973, p. 64.